Marine and Petroleum Geology 28 (2011) 1648–1662

Contents lists available at ScienceDirect

Marine and Petroleum Geology

journal homepage: www.elsevier.com/locate/marpetgeo

Simulating the effect of subseismic fault tails and process zones in a siliciclastic reservoir analogue: Implications for aquifer support and trap definition

Atle Rotevatn [a,b,*], Haakon Fossen [a,b]

[a] Department of Earth Science, University of Bergen, Postboks 7803, 5020 Bergen, Norway
[b] Uni CIPR (Centre for Integrated Petroleum Research), Uni Research, Postboks 7800, 5020 Bergen, Norway

ARTICLE INFO

Article history:
Received 24 January 2011
Received in revised form
26 June 2011
Accepted 11 July 2011
Available online 23 July 2011

Keywords:
Fault tip
Process zone
Prospect evaluation
Fluid flow
Sandstone reservoirs
Reservoir modelling

ABSTRACT

Subsurface, intra-reservoir faults have subseismic portions (the fault tail) and process zones that must be considered for a complete evaluation of their role in a reservoir setting. In this paper we show that this subseismic fault domain, generally associated with all seismically mappable faults, may extend several hundred meters beyond the seismically mapped tip point, depending on vertical seismic resolution and fault displacement gradients along strike. We use reservoir modelling and fluid flow simulation of a sandstone reservoir analogue to demonstrate how a low-permeable process zone may generate steep pressure gradients in the reservoir and affect the tortuosity of reservoir fluid flow. Results and examples combined show how small adjustments in fault interpretations in the subseismic domain may significantly affect trap definition, prospect volumes, project economics and selection of exploration well locations. For production settings, we demonstrate how low-permeable fault tails and process zones may increase flow tortuosity and delay water breakthrough, thereby enhancing sweep efficiency and recovery from otherwise bypassed pockets of hydrocarbons in the reservoir. The results also indicate that process zones may contribute to pressure compartmentalization. Finally, a simple methodology for the estimation of subseismic fault continuity is presented.

1. Introduction

1.1. Fault evolution and generic architectural relationships

Segment growth and linkage is a well accepted paradigm for fault evolution (e.g. Peacock and Sanderson, 1991; Anders and Schlische, 1994; Childs et al., 1995; Cartwright et al., 1996; Cowie et al., 2005). It is also widely recognized that as faults propagate, deformation affects rocks in front of the propagating fault tip (e.g. Cowie and Shipton, 1998). Such deformation may include non-brittle structures such as fault-related folds (e.g. Withjack et al., 1990; Schlische, 1995; Gawthorpe et al., 1997; Kane et al., 2010), but also brittle fractures, micro-faults and deformation bands (e.g. Scholz et al., 1993; McGrath and Davidson, 1995; Fossen et al., 2007). The zone of brittle deformation is manifested as a continuation of the fault itself, known as a 'process zone' (*sensu* Cowie and Shipton, 1998) or 'tip damage zone' (*sensu* Kim et al., 2004), herein referred to as the process zone. Faults propagate radially from a point of initiation (e.g. Marchal et al., 1998), and, consequently, the process zone envelopes the fault plane in all directions (Fig. 1). Structural elements typically found in the process zone include fractures and deformation bands, and previous work has demonstrated that such structures may affect fluid flow in a reservoir (e.g. Caine et al., 1996; Micarelli et al., 2006; Rotevatn et al., 2009b).

1.2. Fault seal

Faults may represent seals or conduits for fluid flow in subsurface reservoirs (e.g. Caine et al., 1996; Knipe, 1997; Fisher and Knipe, 1998; Hesthammer and Fossen, 2000; Fisher and Knipe, 2001; Hesthammer et al., 2002; Harris et al., 2003). Often, faults have contrasting effects on fluid flow, acting as baffles or seals to cross-fault flow while being conduits for along-fault flow (e.g. Aydin, 2000; Shipton et al., 2005). The properties of faults as barriers/conduits for flow are controlled by a number of factors. These can be split into two main categories: 1) juxtaposition and 2) the properties of the fault itself. Juxtaposition of reservoir beds against low- or non-permeable units represents efficient seals (Allan, 1989; Bentley and Barry, 1991; Hoffman et al., 1996; Childs et al., 1997; Knipe, 1997; Sorkhabi and Tsuji, 2005). The properties of the fault itself, which

* Corresponding author. University of Bergen, Department of Earth Science, Postboks 7803, 5020 Bergen, Norway. Tel.: +47 48109959.
E-mail addresses: atle.rotevatn@uni.no (A. Rotevatn), haakon.fossen@geo.uib.no (H. Fossen).

0264-8172/$ – see front matter © 2011 Elsevier Ltd. All rights reserved.
doi:10.1016/j.marpetgeo.2011.07.005

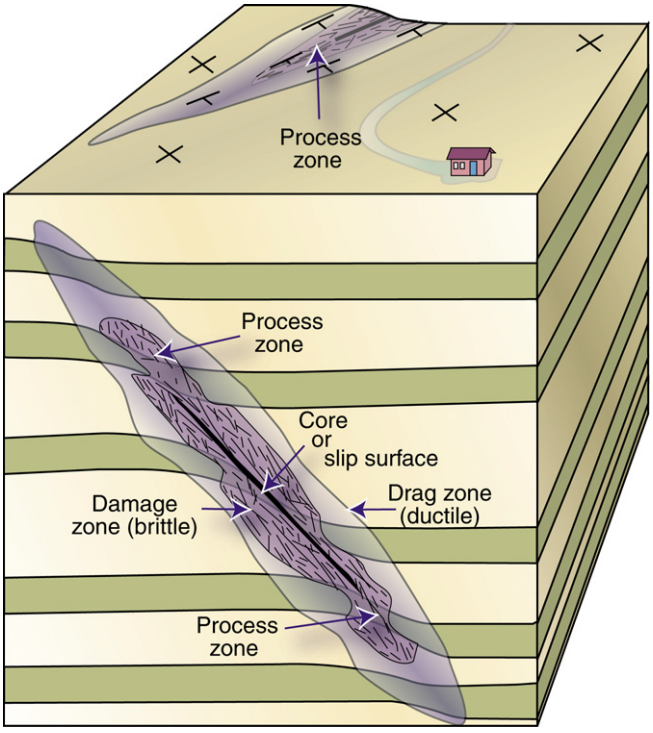

Figure 1. Simplified anatomy of a fault. The damage zone and process zone envelop the fault in three dimensions. Modified from Fossen (2010).

control fluid flow across and along the actual fault, are controlled by the properties of the rock volume affected by tectonic deformation (e.g. Childs et al., 1997; Braathen et al., 2009). The processes controlling such properties include cataclasis (Engelder, 1974; Blenkinsop, 1991), pore collapse during deformation band formation (e.g. Aydin and Johnson, 1978; Antonellini et al., 1994; Fossen and Hesthammer, 1998), clay/shale smearing (e.g. Lindsay et al., 1993; Yielding et al., 1997; Sperrevik et al., 2000; Færseth, 2006), cementation (e.g. Knipe, 1993; Sverdrup and Bjørlykke, 1997; Hesthammer et al., 2002; Fisher et al., 2003), and pressure solution (e.g. Peacock et al., 1998; Bastesen and Braathen, 2010). Whereas these processes may result in structures or membranes that inhibit fluid flow (e.g. clay/shale smears, deformation bands, cementation), other structures formed (e.g. extension fractures, slip surfaces) may represent important fluid conduits (e.g. Evans et al., 1997; Aydin, 2000).

In production flow simulators, fault properties are accounted for by the use of transmissibility multipliers (e.g. Walsh et al., 1998). However, transmissibility multipliers only act on flow perpendicular to the fault, and thus do not capture fault zone permeability anisotropy very well (Manzocchi et al., 1999). Furthermore, assignment of transmissibility multipliers often is a process of 'tuning' faults to match historic production data. As a consequence, history matching becomes the de facto main concern in many fault seal analyses, at the expense of considerations based on geological reality. Although this approach may still result in simulation models that satisfactorily compare with historic data, the fault properties are likely wrong due to the non-uniqueness of the problem when solved this way. This may in many cases be difficult to overcome largely due to data availability and resolution issues, yet evaluating historic production data in light of a more holistic understanding of subsurface structural complexity (i.e. integration between reservoir engineers and structural geologists) is likely to improve the realism in many cases. In geological reality, fault properties depend on the properties of the entire rock volume affected by tectonic deformation (e.g. Caine et al., 1996; Hesthammer and Fossen, 2000; Shipton and Cowie, 2003; Flodin and Aydin, 2004; Berg and Skar, 2005; Johansen et al., 2005; Braathen et al., 2009). This includes the damage zone, which is the volume of deformed rocks enveloping the fault core, resulting from the initiation, propagation, interaction and build-up of slip along faults (Cowie and Scholz, 1992; McGrath and Davidson, 1995; Kim et al., 2004), and which may have significant impacts on fluid flow (e.g. Antonellini and Aydin, 1994; Caine et al., 1996).

1.3. Seismic imaging of faults

Faults in general are too steep to be imaged on seismic data, and their presence is therefore generally detected by the identification of discontinuous, displaced reflectors (lithologic layers). The vertical resolution of seismic datasets constrains our ability to identify geological layers (reflectors) in the stratigraphy; the minimum vertical distance between two features that are possible to define separately rather than as one. This is controlled by the wavelength of the seismic signal; the Rayleigh criterion states that the resolution limit of a reflection is a quarter-wavelength (e.g. Knapp, 1990). For modern, commercial, high-quality 3D seismic data sets this translates to a vertical resolvability of 20–30 m. This defines an approximate lower practical constraint on seismically detectable fault offsets. In reality however, displacement of single strong reflectors may be more easily resolved compared e.g. to the resolvability of vertically stacked beds. For older and less sophisticated datasets vertical resolution can be in the order of 50 to hundreds of meters. Seismic imaging of faults is also complicated by noise as the signal may be scattered and perturbed by the fault (e.g. Hesthammer et al., 2001). This problem increases with geometric complexity of faults which may cause poor and chaotic fault imaging. Processing error, particularly in areas of poor imaging, may also mask fault geometry and lead to geologically unrealistic fault models. Sophisticated processing of high-quality 3D data sets accompanied by advanced geophysical visualization techniques (seismic attribute analysis) has led to giant leaps in fault imaging and interpretation over the past couple of decades, yet imaging of faults will never be better than the basic geophysical dataset itself. The constraints provided by seismic resolution therefore dictate that understanding of subseismic fault features cannot be based solely on seismic data, but must also include considerations based on information from wells (where available) and outcrop analogues.

1.4. Study aims

Previous studies have improved our understanding of fault zones and their effects on reservoir fluid flow (see e.g. review by Faulkner et al., 2010 and references therein), including in recent years a wider understanding of the effect of the damage zone. The effect of the *process zone* on fluid flow, representing the continuation of the damage zone in front of the propagating fault tip (Cowie and Shipton, 1998), has however not to date been covered in the literature. This article takes aim to quantify and describe the potential effects of process zones on fluid flow in subsurface reservoirs. This is achieved through as study of a well exposed outcrop example in the Western USA. An outcrop analogue reservoir modeling study was undertaken and is presented herein in order to investigate the potential impacts of a subseismic process zone. Summarized, the current study aims to:

1. Structurally describe and document an outcrop example of a process zone in Arches National Park, Utah;
2. Investigate the impact of the process zone on fluid flow by means of fluid flow simulation of an analogous reservoir model based on the outcrop;

3. Explore and discuss the implications of subseismic fault elements (fault tails and process zones) for hydrocarbon exploration and production in light of our findings;
4. Present a simple methodology for the prediction of subseismic fault continuity.

2. Datasets

The current study combines structural outcrop data and analogue reservoir modeling data. The outcrop dataset was collected from a fault system dissecting aeolian sandstones of the Jurassic San Rafael Group in SE Utah, USA (Fig. 2), from which spatial data from fault core, damage zone and process zone elements were recorded. The outcrop data have been used as input to analogue reservoir modeling, from which a simulated production and pressure dataset was derived. The current study represents a continuation of work presented in Rotevatn et al. (2009b), where the role of relay ramps as conduits for fluid flow was treated based on data from the same area.

3. Outcrop data, SE Utah

3.1. Geological framework

The study area is situated in the Colorado Plateau of SE Utah, in the Entrada Sandstone of Jurassic San Rafael Group (Fig. 2C). The

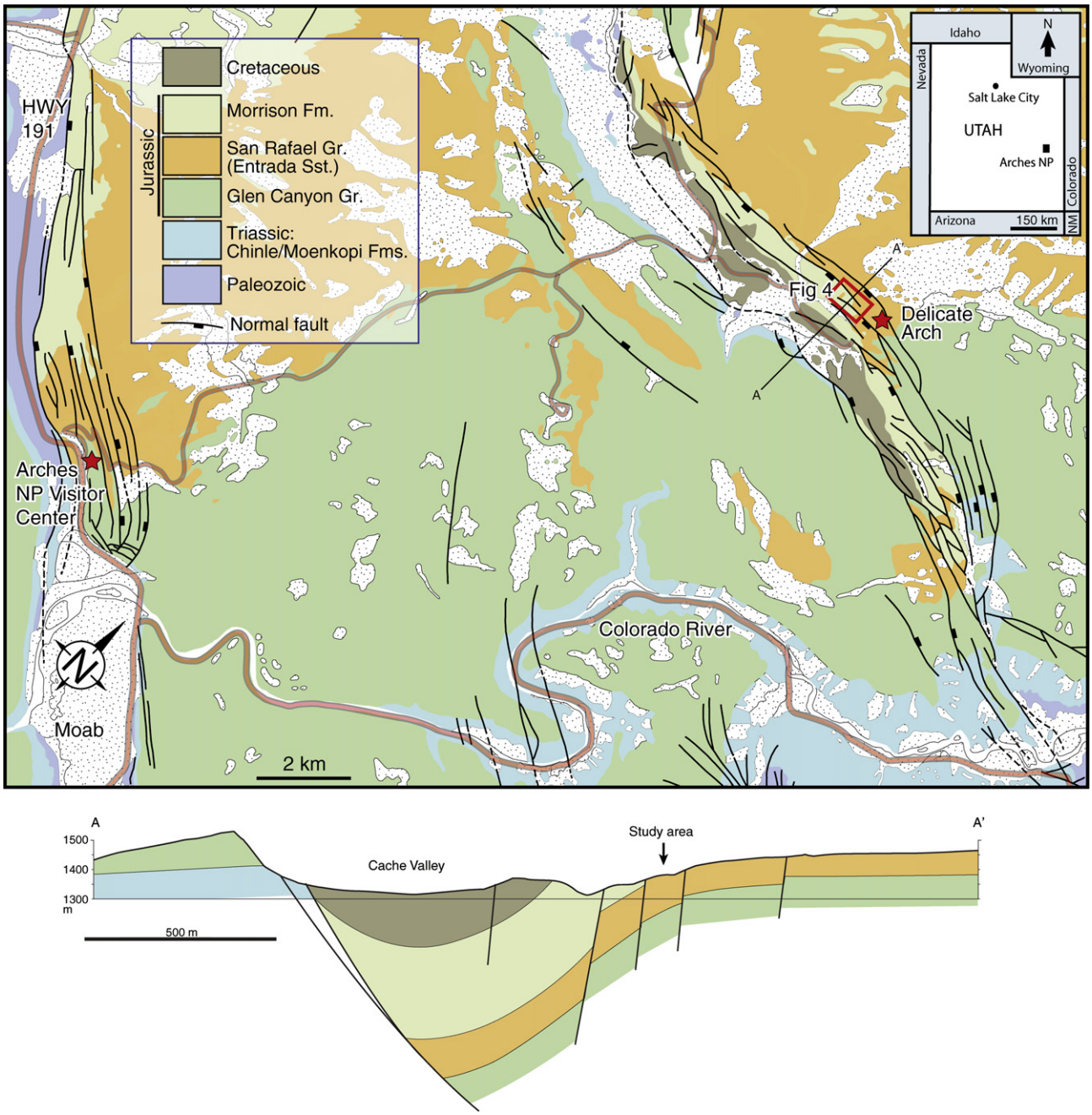

Figure 2. Map of Arches National Park and cross-section from the study area based on Doelling (2001), Antonellini and Aydin (1995). The location of the mapped area in Fig. 4 is shown.

Entrada sandstone is of aeolian origin in the study area and was deposited in a hot and arid coastal desert environment in Callovian (Mid-Jurassic) time (Crabaugh and Kocurek, 1993). A shallow, fluctuating groundwater table controlled by variations in climate, tectonics or sea level (Kocurek et al., 2001) led to cyclic deposition of aeolian dune units and interchangeably wet sabkha deposits. The succession subsequently subsided and was buried by younger deposits during the Cretaceous opening of the Western Interior Seaway. Post-burial, the Jurassic Entrada sandstone was exhumed and brought to its current elevation through the uplift of the Colorado Plateau during the Late Cretaceous Laramide Orogeny (Bump and Davis, 2003) and, subsequently, continued uplift in the Late Cenozoic following a change to shallower subduction angle of the Pacific Plate below North America (Davis, 1999).

The studied fault system is located in Cache Valley, Arches National Park, Utah, affecting the Entrada beds in a roll-over anticline in the hanging wall of a major E-W trending extensional fault system (Fig. 2D). The fault system follows the collapsed crest of the Salt Valley anticline (Fig. 2B), which formed as a response to doming and subsequent collapse of subsurface evaporites of the Pennsylvanian Paradox Formation (e.g. Trudgill, 2010). The age of the faulting in the area is uncertain, but K–Ar (Pevear et al., 1997) and Ar/Ar dating (Solum et al., 2005) indicate fault slip during the late Cretaceous to Early Tertiary (Laramide) time period. This was also the time of maximum burial, implying that faulting of the Entrada Sandstone occurred at burial depths in excess of 2 km (Nuccio and Condon, 1996; Garden et al., 2001). The studied outcrop consists of a c. 80 m sequence of the Entrada Sandstone, featuring a succession of massive mature aeolian dune units (4–20 m thickness), interbedded with fine-grained heterolithic interdune units (1–7 m thick).

Structurally, the outcrops are characterized by extensional faulting and an abundance of cataclastic deformation bands and fault rocks (Antonellini and Aydin, 1994; Antonellini et al., 1994; Antonellini and Aydin, 1995; Cruikshank and Aydin, 1995; Davatzes and Aydin, 2003; Rotevatn et al., 2007), owing to fault evolution through progressive deformation band formation in the porous clastic host rock (*sensu* Aydin and Johnson, 1978). For a review of the literature on deformation of porous sandstones, see Fossen et al. (2007).

A challenge when studying fault tips and process zones is finding outcrops where this part of the fault system is exposed. For the current system we selected a segment of a fault zone located in the north side of Cache Valley, Arches National Park. This choice was made based on the excellent exposure of its fault tip and process zone. The fault segment in question will be referred to as the *Cache fault* in this paper.

3.2. Structural characteristics of the Cache fault

The E-W striking, south-dipping (c. 70°–80°) Cache fault (Fig. 3A) dies out toward the east, where the process zone is found in the continuation of strike of the fault itself. The Cache fault and its core, damage zone and process zone were mapped in detail, and structure (deformation band) frequency profiles were recorded along N-S scanlines (Fig. 4).

The fault core is variable in composition and is characterized by patches of cataclastic fault rock, clusters of deformation bands (some comprising up to an estimated 80–100 bands) and several discrete slip planes with distinct slickenlines (Fig. 5). Fault displacement increases westward from the tip point to >60 m at the end of the mapped section, where it is still increasing (Fig. 3). The fault forms the northern bounding fault of a soft-linked overlap structure or relay ramp (Rotevatn et al., 2007), juxtaposing sandstones from different stratigraphic levels of the Entrada Sandstone. The fault tip is marked by the termination of discrete and detectable offsets. Profiles across the Cache fault (Fig. 4; Profiles A-D) show a peak in structure frequency in and near the fault core, a decline through the hanging- and footwall damage zones into background levels of structure frequency. There is a decline in damage zone width and strain to the east along the fault and process zone (Fig. 4; Profiles A-J). It should be noted that structural background levels are elevated in this area due to the presence of the relay ramp immediately to the south of the Cache fault (Rotevatn et al., 2007).

The process zone is characterized by a surprisingly continuous system of deformation bands (Fig. 4). Near the fault tip, the process zone comprises clusters, each consisting of >40 deformation bands, which split up into smaller clusters and individual deformation bands to the east, i.e. away from the fault tip. Near the termination of the tip damage zone some 350 m east of the fault tip, only a few thin clusters (<10 bands) and individual deformation bands are found. It should be noted that at the fault tip, the tip damage zone steps c. 30 m to the north, from where it continues east along the strike of the main fault.

Displacement was measured and recorded along the length of the Cache fault in the study area. Discrete displacement along slip surfaces as well as displacement along deformation bands in the damage zone were recorded and cumulated to generate total displacement along the fault. The cumulative displacement along deformation bands in the process zone was also recorded. The resulting displacement-length data set from the Cache fault and its process zone is shown in Fig. 3B. Along the fault itself, displacement is taken up as a combination of slip along discrete fault surfaces and shear distributed in deformation bands in the damage zone. In the process zone, displacement is exclusively taken up by deformation bands. The data show how displacement declines near linearly from the west toward the tip point with a gradient of about −0.1. Past the tip point and entering the process zone, the displacement decline is much gentler, at a rate of ∼−0.003 or nearly 2 orders of magnitude less than that of the fault itself.

4. Analogue reservoir modelling and flow simulation

Analogue reservoir modelling is widely used to study the effects of reservoir geometry (e.g. depocentres, facies distribution and bed geometries) or heterogeneity (e.g. flooding surfaces, shale drapes, faults and fractures) to reservoir response (e.g. Dreyer et al., 1993; Stephen and Dalrymple, 2002; Howell et al., 2006; Rotevatn et al., 2009a). The approach allows for high-resolution datasets from outcrop to be incorporated into a model where effects on fluid flow can be studied. Lessons learnt may help improve the understanding of subsurface reservoirs.

4.1. Analogue reservoir model design

In order to quantify the effect of the process zone of the Cache fault on fluid flow, a reservoir model was built and flow simulated based on collected outcrop data. The reservoir model was built following the principles described in Rotevatn et al. (2009b); a short summary is given herein. Roxar's reservoir modelling suite *Irap RMS* was used in this study.

Spatial outcrop data was used as input to build a single-zone geocellular model of the outcrop, incorporating the Cache fault and process zone. Building a relatively small model (c. 1080 m × 680 m × 50 m) allowed for high resolution (10 m × 10 m × 5 m cell size) and computational feasibility without the need for upscaling (73440 cells in the model). To be able to test the effect of the process zone on compartmentalization, the eastern boundary of the model was set close to the process zone tip to force

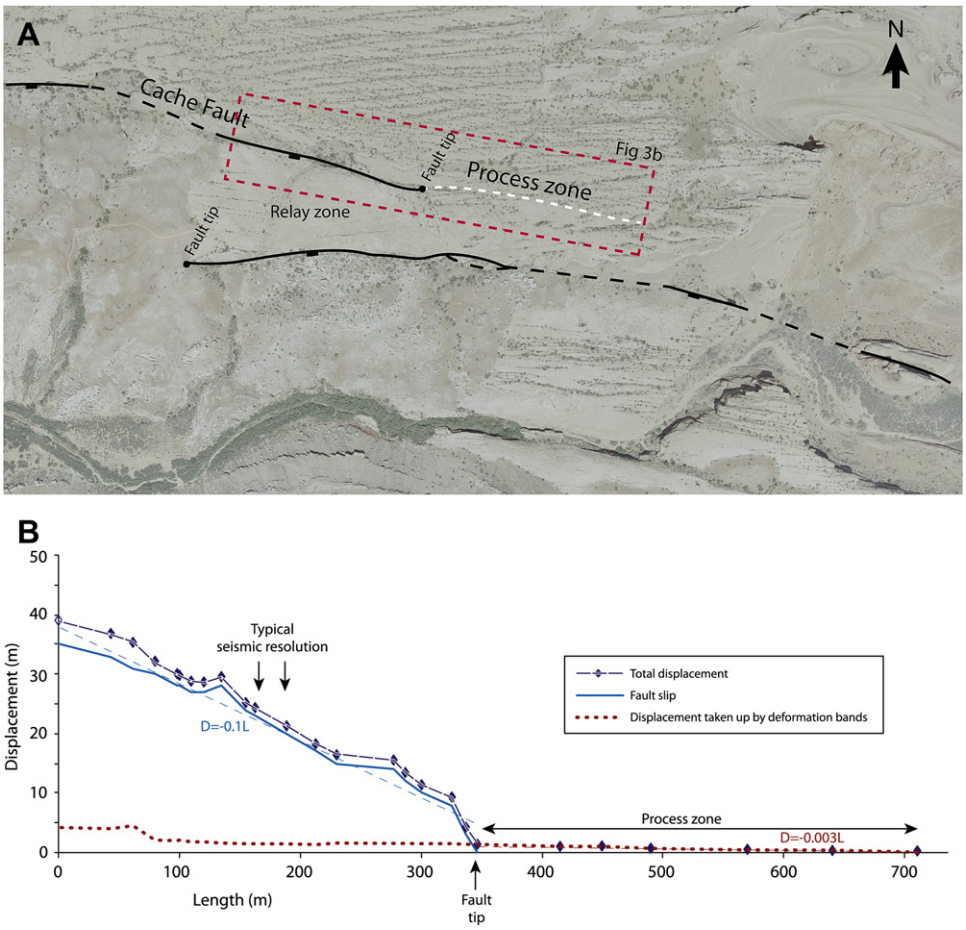

Figure 3. (A) Aerial photo of the study area. The location of the studied Cache fault as well as its fault tip and process zone are shown. The red rectangle indicates the area along which data for the displacement profile in (B) were recorded. (B) Displacement profile along the Cache fault and the process zone beyond the fault tip. Three graphs are shown: discrete fault displacement accommodated by slip surfaces, displacement accommodated by deformation bands, and total displacement. The displacement gradient (D) is shown for the mother fault as well as the process zone, portraying a near 2 magnitude-order difference between the two. (For interpretation of the references to colour in this figure legend, the reader is referred to the web version of this article.)

fluids to cross the process zone during simulation. To isolate the effects of structure, host rock properties (taken from Antonellini and Aydin, 1994) were kept constant throughout the model (porosity 28%; horizontal permeability 1000 mD; vertical permeability 100 mD). Fault planes were implemented discretely using transmissibility multipliers derived analytically (following Manzocchi et al., 1999) based on outcrop and published data (Table 1). Deformation bands mapped in the process zone, damage zone and background were implemented implicitly by modification of grid cell permeability tensors, following the process shown in Fig. 6 and described in detail in Rotevatn et al. (2009b). Deformation band permeability is the key variable to be tested in the modelling and fluid flow simulation part of this study. Values used were in line with published studies (e.g. Antonellini and Aydin, 1994; Fisher and Knipe, 2001; Shipton et al., 2002), using matrix:band permeability contrasts of 10^1, 10^3 and 10^5 in our models.

4.2. Fluid flow simulation

Flow simulation was performed using the RMS finite difference, black oil simulator. The dynamic properties used to condition the models are summarized in Table 2. Typical mid-range properties were used and kept constant for all model runs. The flow simulations were based upon a single vertical water injection well and a single vertical production well placed on opposite sides of the fault system 700 m apart (Fig. 4). Flow rates of 500 Sm^3/day were used for both injector and producer, and a fixed bottom-hole pressure of 300 bar was set for the injector. Simulations were run until water breakthrough occurred in the producing well, but with an upward constraint of 50 years maximum simulation time.

The purpose of the exercise was to use flow simulation as a dynamic test of reservoir response to the presence of structural heterogeneity and perform a comparison of the different model scenarios. More sophisticated simulation approaches and optimization of the production are beyond the scope of this study.

A total of 10 models were built and flow simulated; the key variable being deformation band permeability. Simulation results were used to address the following questions:

1. Does the process zone of the Cache fault contribute to compartmentalization of the reservoir?
2. What are the effects of the process zone on production-related fluid flow?

Key production parameters monitored to analyze model sensitivity to the process zone were pressure and fluid saturation.

4.3. Simulated production data summary

Monitoring reservoir pressure in the model throughout the simulations reveals pressure gradients between the injection- and production wells that steepen with decreasing deformation band

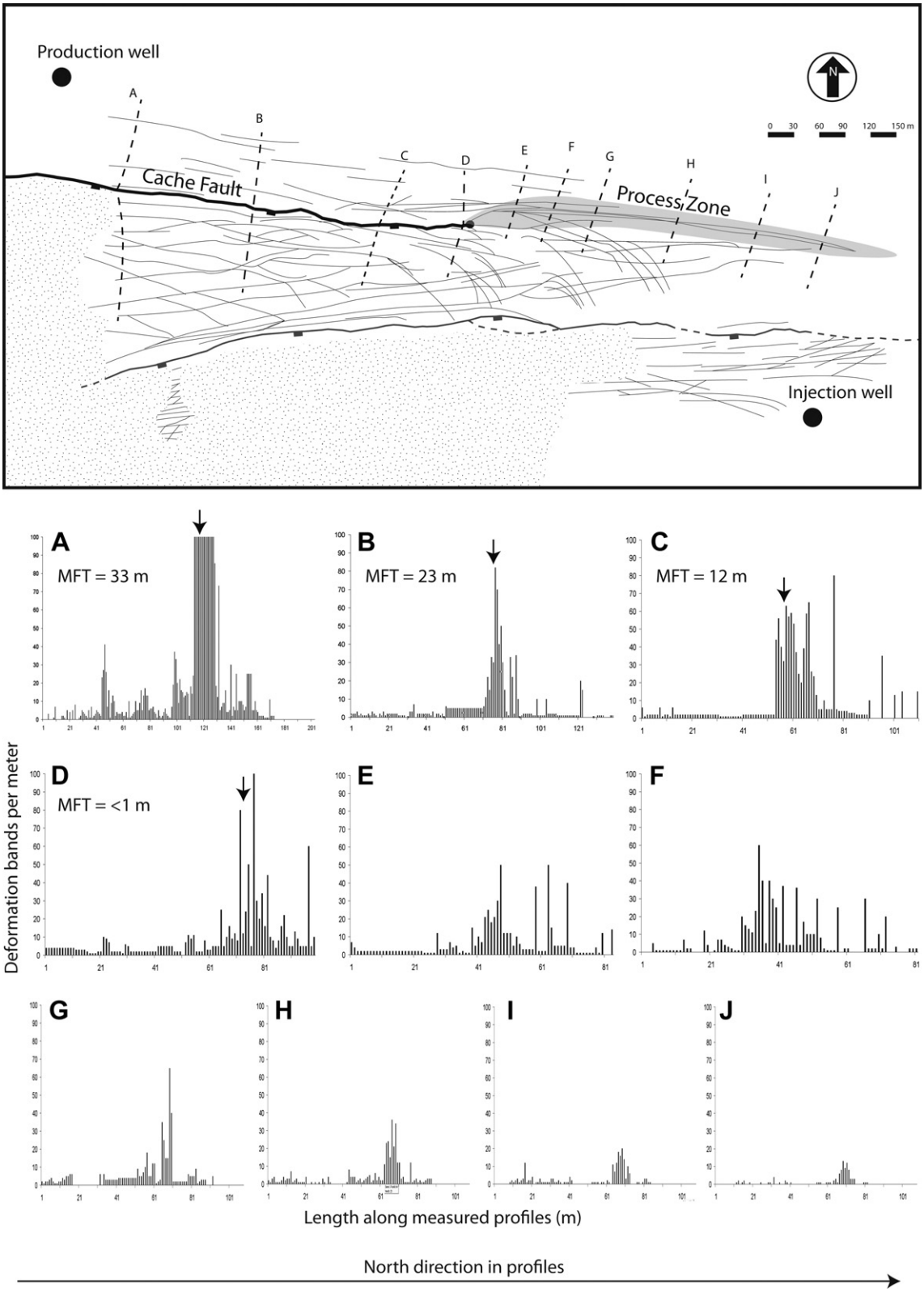

Figure 4. Structural map of the study area showing faults and cataclastic deformation band clusters. The locations of the injection- and production wells used in the analogue reservoir modelling and fluid flow simulations are shown (see section 4 for details). Profiles across the main fault (A–D) and the process zone (E–J) show structure frequency (number of deformation bands per meter). In profiles A-D the position (arrows) and throw of the main fault (MFT = Main Fault Throw) is indicated. The location of the mapped area is shown in Fig. 2.

permeability (Fig. 7). Similarly, pressure changes become more localized to the Cache fault and, perhaps less expectedly, the process zone in the lowest-permeable cases.

In the case of a process zone of extremely low-permeable (permeability contrast of 10^5) deformation bands, there is significant compartmentalization. There is a distinct drop in pressure

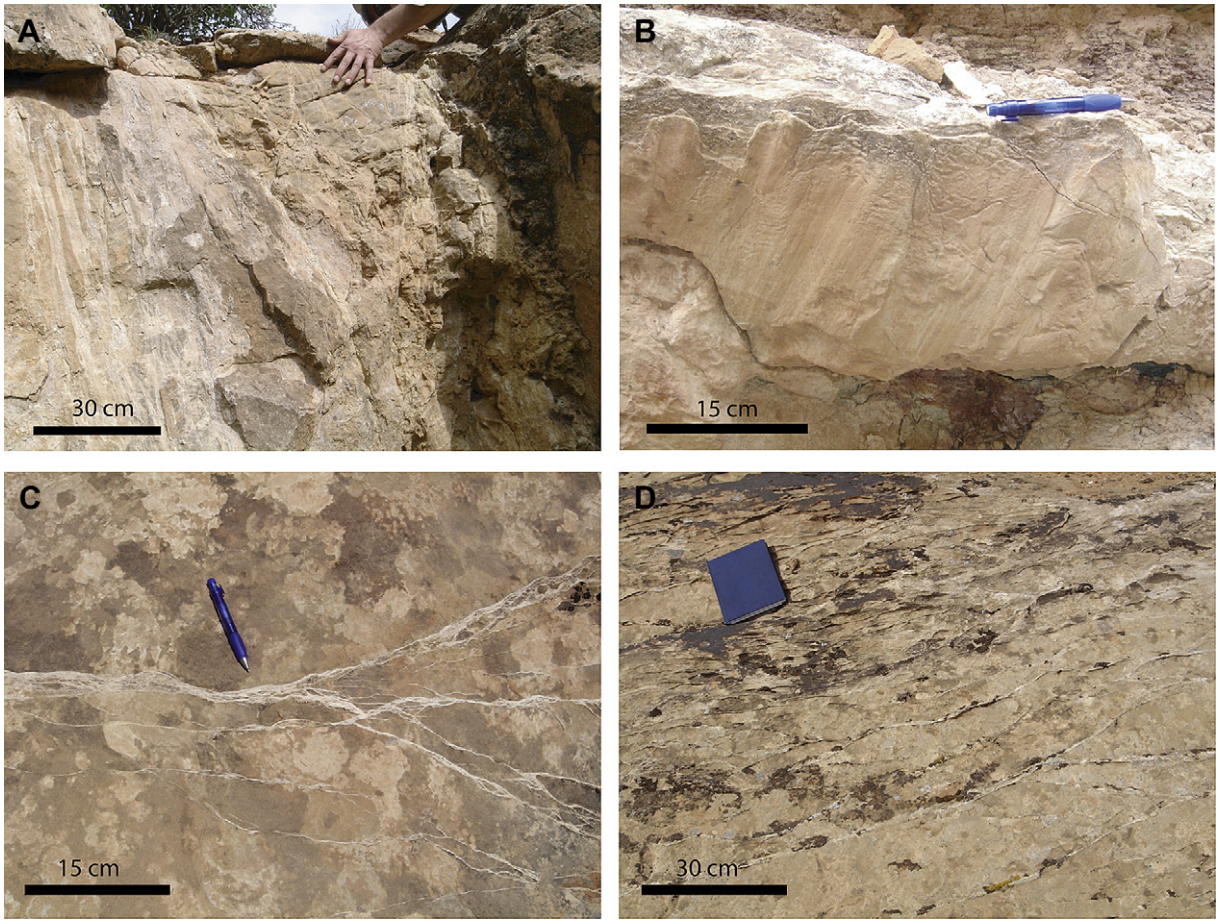

Figure 5. Photographs showing details from the fault core and process zone of the Cache fault (A) In the right-hand half of the photograph, the high-strain fault core is characterized by a combination of discrete slip planes and a ~50 cm wide zone of intensely sheared sand, including clusters of cataclastic deformation bands. The left-hand half of the picture shows the relatively lower-strain inner damage zone, where clusters and individual cataclastic deformation bands can be seen. (B) Slip plane in fault core with slickenlines indicating near dip-parallel slip. (C) Cataclastic deformation bands in the process zone, with individual bands coalescing into deformation band clusters. (D) Network of cataclastic deformation bands and clusters in the damage zone.

across the process zone of up to 50 bar over a very short distance, creating two distinct pressure compartments on each side of the Cache fault process zone (Fig. 8).

In the examples where permeability contrast is lower (10^1 and 10^3), pressure drops are more gradual and the pressure compartmentalization less significant (Fig. 7).

Oil saturation results (Fig. 9) demonstrates differences in how injection fluid (water) displaces oil from the injector to the producer. In the high-permeability case (Fig. 9C) fluids choose the most direct path between the injector and the producer, seemingly unaffected by the process zone. Decreasing permeability of deformation bands in the process zone leads to increasingly tortuous flow, with injection fluids travelling further east along strike in order to flow 'around' the fault and process zone (Fig. 9A–B). The result of the contrasting flow tortuosity between the models is seen in Fig. 9 as *a pocket of unrecovered oil* in the north-eastern part of the model. The higher the permeability, the less tortuous the flow of injection fluids, and, thus the larger the pocket of unrecovered oil in the northeast.

5. Discussion

5.1. Displacement gradients in and near the subseismic domain

The understanding and prediction of geological features below seismic resolution is a persistent challenge for geoscientists and engineers in the oil and gas industry. Seismically mappable faults are elusive as there are always elements of them that fall below seismic resolution. This includes the fault tail and the process zone (Fig. 10): the *fault tail* is the part of the fault between the seismically apparent fault tip and the *actual* tip point, whereas the *process zone* is the zone of brittle deformation ahead of the (propagating) main fault tip (Fig. 10). It should be stressed that the term fault tail does not refer to a distinct architectural element of any fault, but is solely related to imaging (i.e. the part of the fault not imaged on seismic). The length of the fault tail therefore depends on the vertical resolution of the seismic data set as well as the rate at which displacement declines toward the fault tip (displacement gradient).

The studied example in SE Utah portrays an abrupt change in displacement gradient between the discrete fault itself (−0.1) and its process zone (−0.003). This demonstrates that along a single fault, magnitude-order changes in displacement gradients may occur that complicate the prediction of fault length at the subseismic scale. We suggest that the observed abrupt change in displacement gradient at the tip point is related to the different processes taking place in the process zone vs. the actual fault. Faults evolve in porous sandstone through the growth of an incipient proto-fault of deformation band clusters, which eventually ruptures as slip patches nucleate, grow and amalgamate to form a through-going slip surface. The pre-rupture process of deformation band cluster growth continues in the process zone ahead of the propagating fault tip. Thus, whereas displacement along the fault

Table 1
Input parameters and analytical determination of fault permeability and fault transmissibility multipliers.

Parameter	Explanation	Value	Comments
t_f	fault (core) thickness	1 m	
L	grid cell length	10 m	
k_m	grid cell permeability	15 mD	harmonic average of permeability in adjacent grid cells[a]
k_f	fault permeability	0.161 mD	derived from below
T	*Fault transmissibility multiplier*	*0.10*	calculated using Manzocchi et al. (1999)
k_f above is the harmonic average permeability of the fault core based on the following input:			
l_1	accumulated thickness of 100 deformation bands	0.2 m	
k_1	deformation band permeability	1 mD	the median of permeability values used in our models
l_2	accumulated thickness of three slip planes	0.006 m	three slip planes are used as an average
k_2	slip plane permeability	0.001 mD	based on Antonellini and Aydin (1994)
l_3	host rock thickness (L_{tot} minus l_1 and l_2)	0.794 m	
k3	host rock permeability	1000 mD	the host rock permeability used in all our models
L_{tot}	total thickness	1 m	
k_f	*fault permeability*	*0.161 mD*	resulting harmonic average permeability of fault core

[a] Based on our mapping, the average values of deformation bands per meter in the grid cells adjacent to the main faults range mainly between 21 and 100 deformation bands per meter. Using the median of deformation band permeabilities used in the models (1 mD), this gives a grid cell harmonic average permeability of 15 mD. This value represents the average of several calculations using different numbers of bands per meter in the range 21–100.

itself is largely taken up by discrete slip on slip surfaces, with a subordinate component of displacement accommodated by deformation bands in the damage zone, the process zone accommodates displacement through deformation band formation only. Deformation bands are inherently different from slip surfaces, which are weak and tend to accumulate more displacement in subsequent slip events (strain softening). Deformation bands are mechanically strong (strain hardened; e.g. Kaproth et al., 2010) and additional displacement accumulate by the formation of new deformation bands rather than by reactivation of existing bands (Aydin and Johnson, 1978). Single cataclastic deformation bands reportedly exhibit a logarithmic D_{max}–L relationship with an exponent of ~0.5 (Fossen and Hesthammer, 1997). This is significantly less than what has been reported for most fault populations, where the exponent tends to be close to 1.0 (e.g. Walsh and Watterson, 1988; Marrett and Allmendinger, 1991; Dawers et al., 1993; Schlische et al., 1996). Additionally, deformation bands may exhibit low D/L ratios, particularly when allowed to propagate unrestrictedly, i.e. when their tips are not blocked by pre-existing structures (Wibberley et al., 2000). The differences in the way that slip surfaces (faults) and deformation bands accumulate displacement with respect to length is shown here to have dramatic consequences for the fault tip region, where the displacement gradient of the process zone (Fig. 3B) is nearly 2 orders of magnitude less than that of the main fault. It is an important observation that these variations take place along a single fault and its process zone, as these results has implications for understanding the subseismic extent of faults based on seismic data and their influence on reservoir compartmentalization and fluid flow.

5.2. Fault interaction and the process zone

Fault branch points and overlap zones are known to be considerably more complex than single faults (e.g. Shipton and Cowie, 2003; Fossen et al., 2005). Interacting faults are generally associated with a widened damage zone and a great variability of orientation of structural elements. Fault interaction is important also in the context of the process zone. In areas of fault overlap, the perturbation of the local stress field around the interacting faults is known to cause one or both faults to 'turn' toward the other (Fig. 11). At early stages of fault overlap this may not be evident from seismic as it is the fault tail and process zone that will initiate the turn (Fig. 11A). Furthermore, in a situation where a soft-linked relay ramp is inferred from seismic data, the fault tail and process

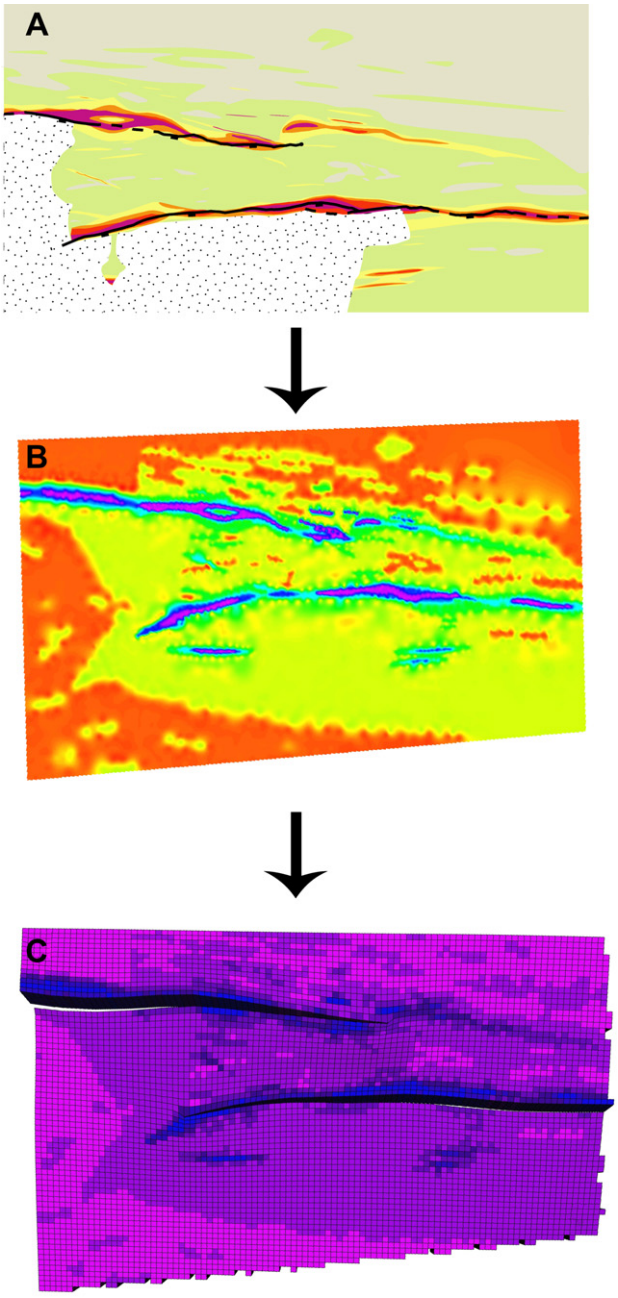

Figure 6. Workflow showing the incorporation of mapped outcrop data into a geocellular model. A deformation band frequency map (A) generated based on mapping presented herein and supplemented by data from Rotevatn et al. (2007) was digitized and imported to the reservoir modelling software as a trend map (B). Subsequently, the trend map was used to populate a 3D trend parameter (C) that was used to condition grid cell permeabilities in the simulation models.

Table 2
Flow simulation dynamic properties.

Length of run	Until water breakthrough in production well	
Other run constraints	Maximum 50 years runtime	
Report Step	1 quarter	
Rock Compressibility	0.0000435 1/bar	
Rock reference pressure	275.79 bar	
Spec. gravity oil	0,8	
Gas/Oil ratio	142.486 sm^3/sm^3	
Corey exp	Water	4
	Oil – water	3
Saturation end points	Sorw	0,2
	Swcr	0,2
Rel. Perm. end points	kromax	1
	krw	0,4
OWC capillary pressure		0
Reference Pressure	100 bar	
Wells	Injectors	1
	Producers	1
Flow Rate	Injector	500 Sm^3/day
	Producer	500 Sm^3/day
Bottom hole pressure	Injectors	300 bar
Initial oil in place	Relay grid	3755514 Sm^3

zone may be hard-linked (Fig. 11C). Other uncertainties may arise in the seismic interpretation of fault networks in scenarios of single-tip fault interaction (*sensu* Fossen et al., 2005), where it may be difficult to determine whether two faults are conjoined or not in contact with one another (the implications of which are discussed in section 5.4).

5.3. Implications for hydrocarbon production

From the flow simulation results presented above it is evident that the process zone is well capable of affecting production-related fluid flow in the reservoir. This is, however, clearly dependent on the properties of the structural heterogeneities within it. Whereas little or no disturbance of fluid flow was inflicted by deformation bands with a small permeability reduction, effects were detected when intermediate- to low-permeable deformation bands were present. Steep pressure gradients with up to 50 bar pressure difference were seen across the low-permeable process zone. This demonstrates that the process zone is capable of contributing to reservoir compartmentalization beyond the termination of the actual fault itself. It should be noted that the observed effects would be even greater where heavier oils are present, as phase and viscosity will heighten the effect of the permeability reduction on flow.

In the production phase, anticipated reservoir compartmentalization affects the planning of production strategies. Understanding reservoir compartmentalization is critical to employ the best possible measures in reservoir stimulation, including the supply of pressure support through optimal placement of injection wells. The fluid flow simulation results herein demonstrate that the fault tail and process zone may contribute to create pressure compartments the reservoir over the time of production. It is therefore necessary to address the subseismic continuation of intra-reservoir faults continuously in the planning phase and throughout field life. Integrated work by production geoscientists and reservoir engineers is therefore paramount to continuously re-evaluate fault

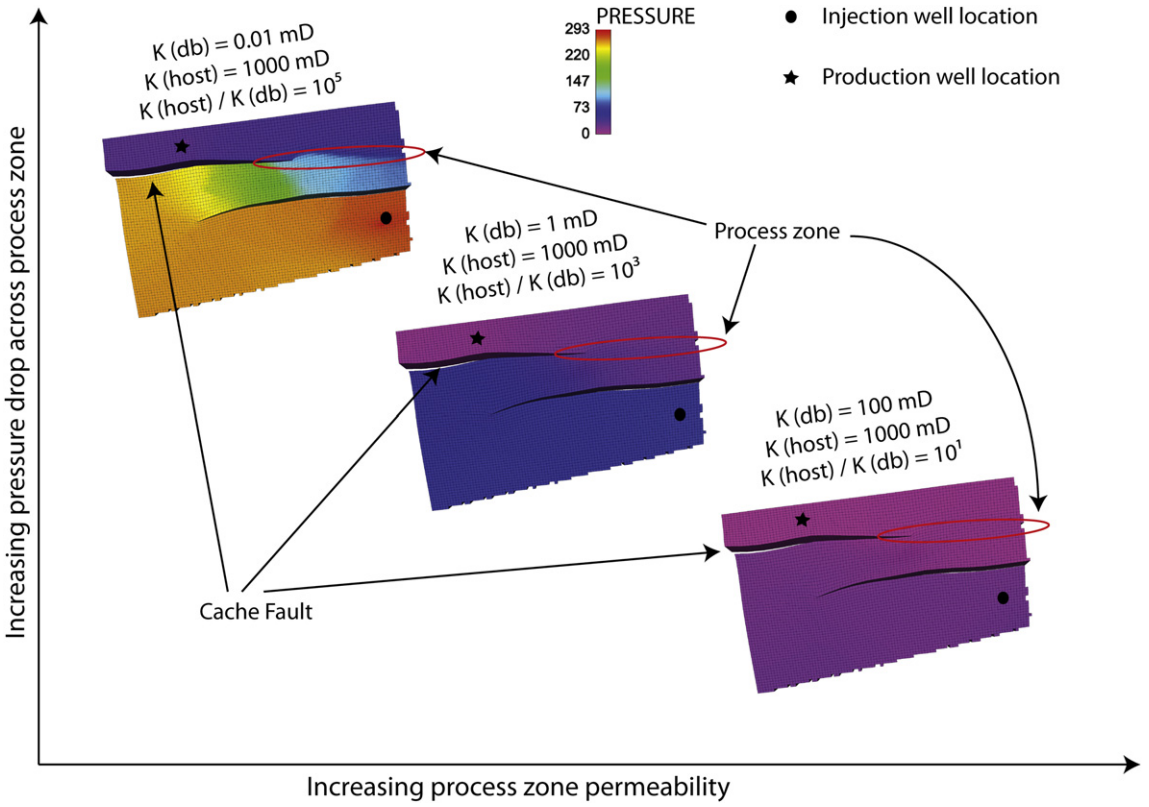

Figure 7. Schematic diagram showing the relationship between the pressure gradient observed across the process zone (red ellipse) and the process zone permeability in each model. The reservoir pressure at the end of simulation runs is shown for each of the models. We observe a decrease in pressure drop across the process zone with increasing process zone permeability. The steepest pressure gradients are thus generated by the lowest permeable process zone. K(db) is the permeability deformation bands (constituting the damage zone and process zone in the model); K(host) is the host rock permeability. The locations of the injection and production wells are shown. (For interpretation of the references to colour in this figure legend, the reader is referred to the web version of this article.)

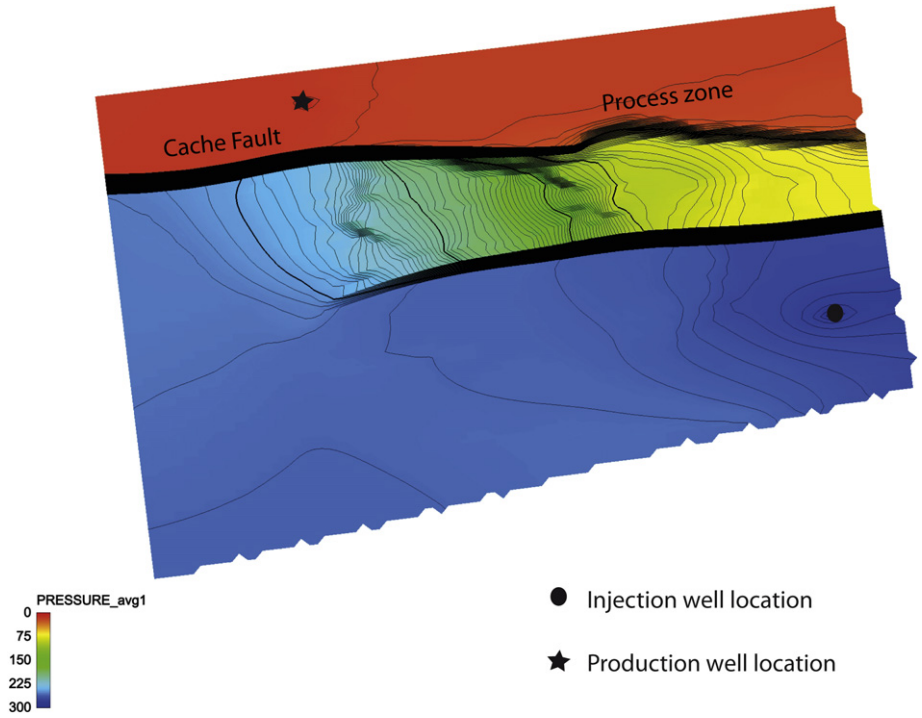

Figure 8. Pressure data shown on depth surface from the middle of the reservoir model. The model shown features the lowest permeable realization of the process zone (as in the upper left model of Fig. 7). Colour scheme and contour lines display pressure at the end of the simulation run, portraying a steep pressure gradient across the process zone. The pressure difference across the process zone is ~70 bar. As the model has sealing boundary conditions this arguably is an artefact of the process zone being in contact with the boundary of the model. However, this can be considered the equivalent of a situation where a process zone is in contact with a sealing fault where the boundary of the model currently is. (For interpretation of the references to colour in this figure legend, the reader is referred to the web version of this article.)

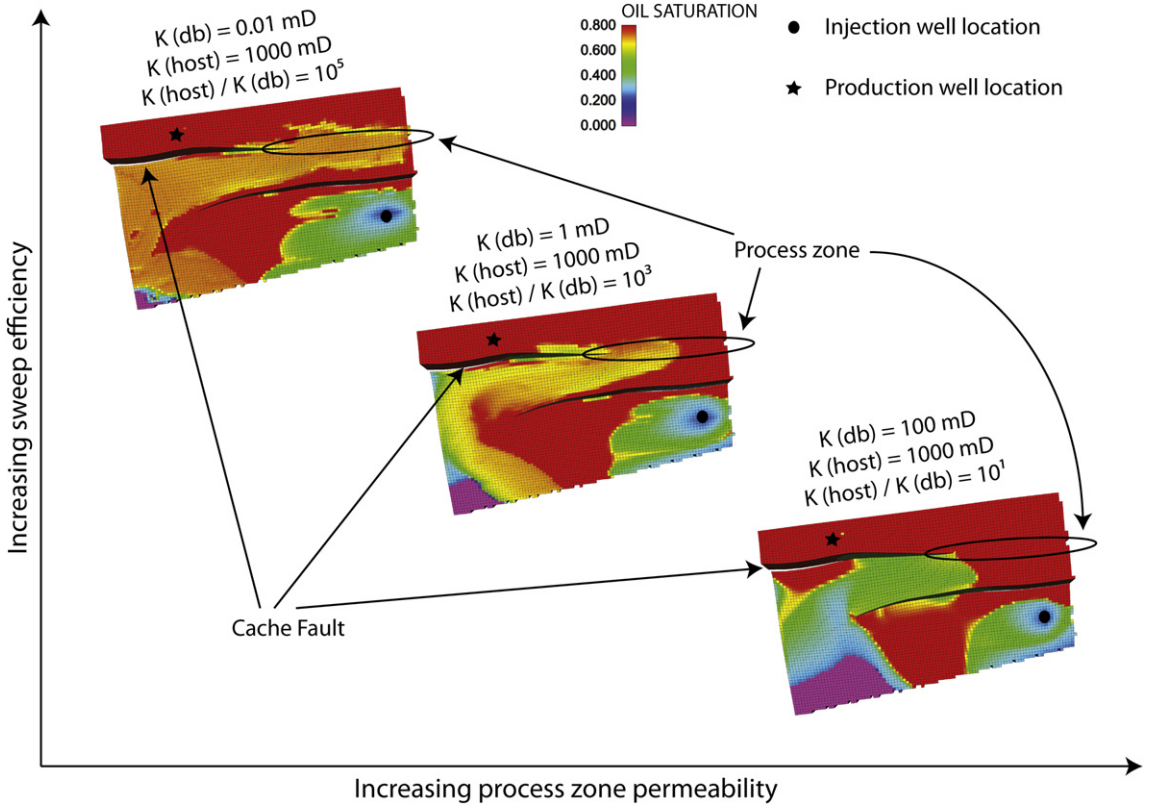

Figure 9. Schematic diagram showing the relationship between sweep efficiency and process zone permeability in each model. The oil saturation at the end of simulation runs is shown for each of the models. It is clear that the upper right corner of t he models is more efficiently swept in the lower permeable models due to the low-permeability process zone forcing injection fluids further east (right). K(db) is the permeability deformation bands (constituting the damage zone and process zone in the model); K(host) is the host rock permeability. The locations of the injection and production wells are shown.

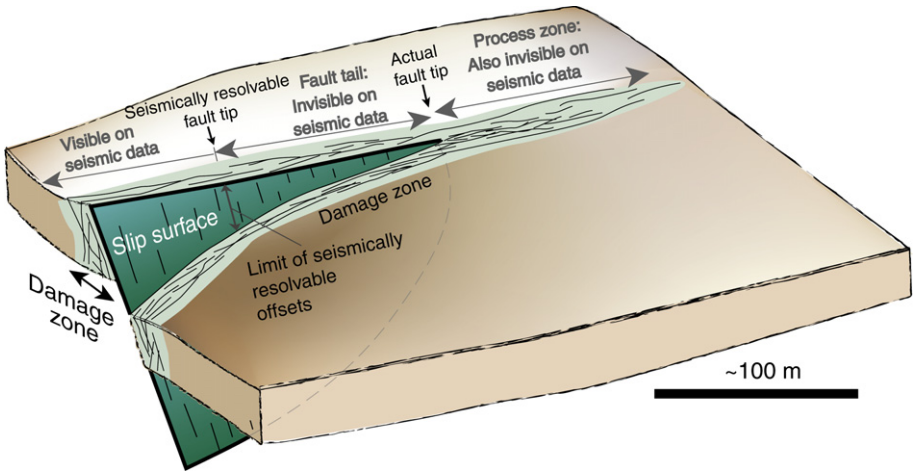

Figure 10. Schematic fault architecture showing the fault plane and the damage- and process zones enveloping the fault. The diagram highlights the portion of the fault that falls below seismic resolution. These include the fault tail, which is the part of the fault between the seismically mapped fault tip and the actual fault tip, and the process zone, which is the zone of brittle deformation ahead of the (presently or formerly propagating) fault tip.

interpretations and improve reservoir models in order to optimize production and enhance recovery.

The perhaps most interesting observation made from our results is that the permeability of the process zone is also controlling the tortuosity of the reservoir fluid flow. In the intermediate- to low-permeability cases injection fluids travel farther east along the strike of the process zone before gradually breaking through to the northern compartment. This also affects sweep efficiency as the increased tortuosity ensures that a larger portion of the reservoir is swept by injection fluids. Increased flow tortuosity and sweep efficiency may delay water breakthrough and increase recovery efficiency. In this case, therefore, structural heterogeneity in the reservoir (represented by the deformation bands in the process zone) arguably has positive effects on production. Early water breakthrough is a great concern of development engineers. Aquifer support over a larger area caused by low-permeable structural heterogeneity as shown herein is therefore an important result with relevance for appraisal and development projects.

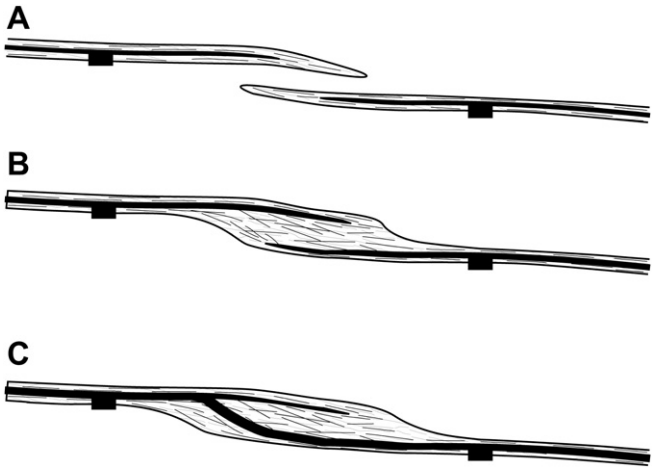

Figure 11. Development of damage zone within and around overlapping fault segments during fault growth. Three stages are shown, from initial overlap of the process zones (A) to a soft-linked relay ramp with overlapping fault segments and a well developed linking damage zone (*sensu* Kim et al., 2004) (B), and finally a breached relay (Trudgill and Cartwright, 1994) where the two segments coalesce (C).

5.4. Implications for hydrocarbon exploration

The fluid flow simulations presented herein are on a production time scale. Fault seal over geological time in a migration perspective is therefore beyond the scope of the current study. Nonetheless, some of the aspects of understanding subseismic fault length may be extrapolated to shed light on issues related to uncertainties associated with trap definition in hydrocarbon exploration and prospect analysis.

In fault-controlled structural traps, understanding the subseismic continuation of a seismically mappable fault may be critical to accurately estimate prospect volumes. Marginal exploration projects, such as smaller structures targeted in mature areas, are particularly sensitive as small changes in fault length may be the difference between an economic vs. a sub-economic prospect. It is useful to present a generalized example of a fault-controlled exploration prospect to illustrate the impact of different interpretations of fault continuity and seal on estimated prospect volumes. In the fault model shown in Fig. 12A, the intersection between faults 2 and 3 appears to be open. However, due to the limitations in seismic resolution, it is not known if this is the case or if the faults actually join and seal the intersection. Fig. 12B shows the consequence of the sealed intersection where hydrocarbon charge from the south fills up a fault-controlled trap south of the fault junction. Fig. 12C shows the alternative, where the open junction allows for a larger prospect to be filled, controlled by dip closure against the sealing faults 1 and 2. In this example it is clear that the selection of an exploration well location depends on the fault interpretation. As prospect volumes (and therefore economics) are also affected, (mis-)interpretation of trap definition may in marginal cases be the difference between an exploration well being drilled or not.

5.5. Risk mitigation

The lack of visual control on subsurface features below seismic resolution clearly represents a risk, technically as well as commercially. The risk can be mitigated through appreciation of fault growth processes and application of technology. For those geologists working with subsurface data who are not specialized in structural geology, the concept of the process zone is probably less familiar than the subseismic part of the actual fault (the fault tail). Both are important as demonstrated by the flow simulation results in this study.

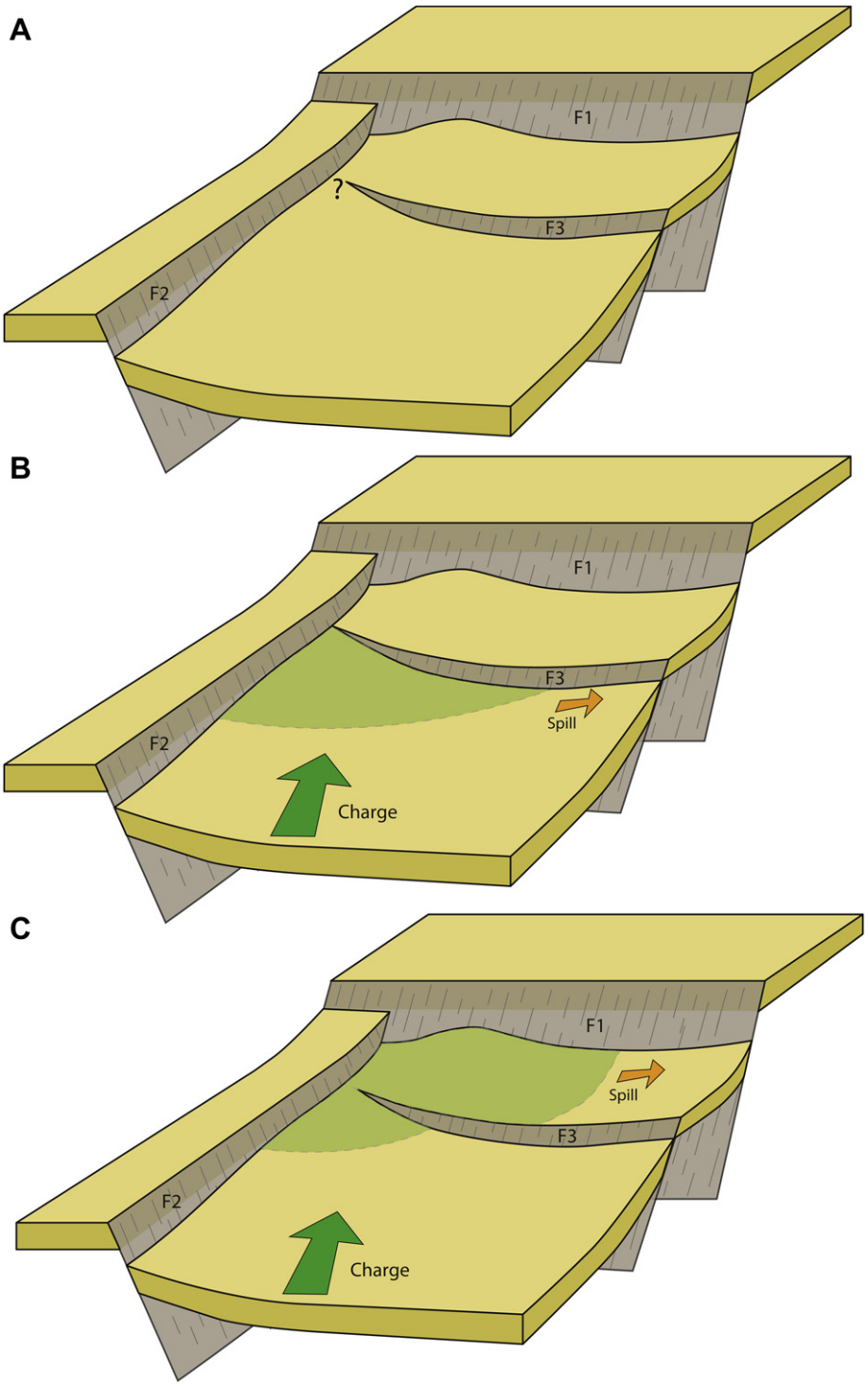

Figure 12. Generalized hypothetical example of a subsurface fault-controlled exploration prospect, highlighting the implications of different fault interpretations for prospect definition. The first figure (A) shows the uncertainty of the contact relationship between faults 2 and 3, which cannot be differentiated based on seismic data. Figures (B) and (C) show two alternative interpretations of the fault junction. It is evident that the two interpretations have different implications for trap definition and prospect volumes, which in turn affect project economics as well as the selection of an ideal exploration well location. See text for details.

By laterally mapping fault displacement from seismic data, a displacement gradient may be established that can be used to estimate the length of the fault tail. The displacement gradient may be estimated by constructing fault displacement diagrams. The seismic fault tip will be the point at which the fault displacement falls below seismic resolution. Fault displacement at this point may be estimated to be equal to the seismic resolution of the dataset. The rate of displacement decline may be extracted from the displacement diagrams (such as in Fig. 3B) constructed from seismic. By applying the rate of decline to the magnitude of displacement at the seismic fault tip (equal to vertical seismic resolution), the distance to the actual fault tip may be estimated. As many displacement profiles exhibit an approximately linear decline (or slightly increasing displacement gradient) toward the tip

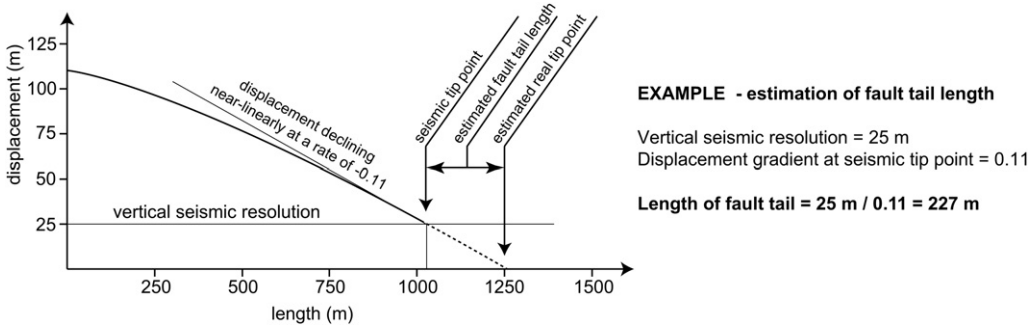

Figure 13. Generic hypothetical example of a displacement diagram mapped from seismic data, illustrating a simple calculation of the subseismic fault tail length beyond the seismically resolvable tip point.

(Cowie and Shipton, 1998), the length of the fault tail may be predicted. A generic example of how this can be done is shown in Fig. 13.

Estimating the length of the ensuing process zone is less straightforward, but the outcrop example showed herein demonstrates that it can endure for several hundred meters beyond the actual fault tip. The length of the process zone is less predictable as it depends on a number of factors, notably lithological factors such as porosity, grain size, grain sorting and cementation of the host rock, but also the local state of stress and fault tip interaction. These factors are not well understood and the current dataset is the only one that quantifies the displacement gradient of a natural process zone (Fig. 3B). An important point to be made is that the length of the process zone does not directly depend on the size of the fault. Cowie and Shipton (1998) suggested that the size of the process zone is expected to scale with the size of the slipping patch during each single fault slip event. Based on this, small and large faults should show similar process zone sizes and properties for any given host rock and structural setting. However, other authors (Cocco and Bizzarri, 2002) have argued that earthquake slip patch size scales with fault length, which would imply some degree of scale dependence between process zone length and fault length. However, this has to date not been fully examined in porous sandstones and therefore remains uncertain and a potential focus for future study.

It is clear that more research is needed to provide constrains on displacement gradients and the scaling of process zone attributes in order to better this understanding. Nevertheless, the example provided herein and known scaling relations for single deformation bands (Fossen and Hesthammer, 1997) indicate that displacement gradients in the process zone will be orders of magnitude lower than those of discrete faults.

6. Summary and conclusions

Outcrop data, analogue reservoir modeling and fluid flow simulation results have been presented to investigate the effect of subseismic fault tails and process zones on reservoir compartmentalization and fluid flow. The most significant observations, conclusions and implications are summarized below:

- The length of the *fault tail* (Fig. 10) may be estimated based on knowledge of the vertical seismic resolution and construction of fault displacement diagrams.
- The *process zone* (Fig. 10) of faults in porous sandstones may extend for several hundred meters past the tip point of the mother fault.
- Process zones show a much lower gradient of displacement decay than does the main fault. The displacement gradients observed in the current study were nearly 2 orders of magnitude less in the process zone compared to the main fault.
- Low-permeable structural heterogeneity may contribute to enhanced aquifer support in subsurface reservoirs and may thus have a positive effect on production. This is clear from the example modeled and flow simulated in the current study, where lowering deformation band permeability led to improved sweep efficiency and recovery by increasing the tortuosity of injection fluid flow and delaying water breakthrough.
- A process zone may represent a significant baffle to fluid flow if comprised of sufficiently low-permeable structural elements (such as the deformation bands of the current study). This may segregate reservoir beds into pressure compartments during production. The deformation bands in the process zone in the current study show a high degree of lateral continuity and interconnectedness. Other examples have highlighted that great variability exists in terms of thickness, continuity and permeability of deformation bands (Fossen and Bale, 2007), and such variations will exercise strong controls on the effect of deformation bands on fluid flow.
- Understanding the total length of a fault system (including fault tail and process zone) is important to correctly understand prospect definition and size in exploration. Prospect volumes control project economics, and small changes in fault interpretation may thus be the difference between a commercial and a sub-commercial prospect.
- Correct trap definition is also crucial for selecting optimal exploration (and production) well locations.

Acknowledgements

Thanks are due to the U.S. National Park Service for permission to conduct research inside Arches National Park. Roxar Software Solutions (now Emerson Process Management) are thanked for the provision of academic licenses for the Roxar RMS. Tor E. Aas is thanked for assistance in the field. Jan Tveranger and John Howell are gratefully acknowledged for engaging in enlightening discussions that helped the reservoir modeling aspects of this study. Two anonymous reviewers are thanked for their constructive and thoughtful reviews which greatly improved the clarity of this paper.

References

Allan, U.S., 1989. Model for hydrocarbon migration and entrapment within faulted structures. AAPG Bulletin 73, 803–811.
Anders, M.H., Schlische, R.W., 1994. Overlapping faults, intrabasin highs, and the growth of normal faults. Journal of Geology 102, 165–180.
Antonellini, M., Aydin, A., 1994. Effect of faulting on fluid flow in porous sandstones: petrophysical properties. AAPG Bulletin 78 (3), 355–377.
Antonellini, M., Aydin, A., 1995. Effect of faulting on fluid flow in porous sandstones: geometry and spatial distribution. AAPG Bulletin 79 (5), 642–671.

Antonellini, M., Aydin, A., Pollard, D.D., 1994. Microstructure of deformation bands in porous sandstones at Arches National Park, Utah. Journal of Structural Geology 16 (7), 941–959.
Aydin, A., 2000. Fractures, faults, and hydrocarbon entrapment, migration and flow. Marine and Petroleum Geology 17, 797–814.
Aydin, A., Johnson, A.M., 1978. Development of faults as zones of deformation bands and as slip surfaces in sandstone. Pageoph 116, 931–942.
Bastesen, E., Braathen, A., 2010. Extensional faults in fine grained carbonates - analysis of fault core lithology and thickness-displacement relationships. Journal of Structural Geology 32, 1609–1628.
Bentley, M.R., Barry, J.J., 1991. Representation of fault sealing in a reservoir simulation: cormorant block IV UK North Sea. In: 66th Annual Technical Conference and Exhibition of the Society of Petroleum Engineers. Texas, Dallas, pp. 119–126.
Berg, S.S., Skar, T., 2005. Controls on damage zone asymmetry of a normal fault zone: outcrop analyses of a segment of the Moab fault, SE Utah. Journal of Structural Geology 27 (10), 1803–1822.
Blenkinsop, T.G., 1991. Cataclasis and processes of particle size reduction. Pageoph 136 (1), 59–86.
Braathen, A., Tveranger, J., Fossen, H., Skar, T., Cardozo, N., Semshaug, S.E., Bastesen, E., Sverdrup, E., 2009. Fault facies and its application to sandstone reservoirs. AAPG Bulletin 93 (7), 891–917.
Bump, A.P., Davis, G.H., 2003. Late Cretaceous-early Tertiary Laramide deformation of the northern Colorado Plateau, Utah and Colorado. Journal of Structural Geology 25, 421–440.
Caine, J.S., Evans, J.P., Forster, C.B., 1996. Fault zone architecture and permeability structure. Geology 24, 1025–1028.
Cartwright, J.A., Mansfield, C.S., Trudgill, B.D., 1996. Fault growth by segment linkage. Special Publications. In: Buchanan, P.C., Nieuwland, D.A. (Eds.), Modern Developments in Structural Interpretations, vol. 99. Geological Society, London, pp. 163–177.
Childs, C., Walsh, J.J., Watterson, J., 1997. Complexity in fault zone structure and implications for fault seal prediction. In: Møller-Pedersen, P., Koestler, A.G. (Eds.), Hydrocarbon Seals: Importance for Exploration and Production, vol. 7. Norwegian Petroleum Society, pp. 61–72. Special Publication.
Childs, C., Watterson, J., Walsh, J.J., 1995. Fault overlap zones within developing normal fault systems. Journal of the Geological Society, London 152, 535–549.
Cocco, M., Bizzarri, A., 2002. On the slip-weakening behavior of rate- and state dependent constitutive laws. Geophysical Research Letters 29 (11), 1516.
Cowie, P.A., Scholz, C.H., 1992. Physical explanation for the displacement-length relationship of faults, using a post-yield fracture mechanics model. Journal of Structural Geology 14, 1133–1148.
Cowie, P.A., Shipton, Z.K., 1998. Fault tip displacement gradients and process zone dimensions. Journal of Structural Geology 20, 983–997.
Cowie, P.A., Underhill, J.R., Behn, M.D., Lin, J., Gill, C.E., 2005. Spatio-temporal evolution of strain accumulation derived from multi-scale observations of Late Jurassic rifting in the northern North Sea: a critical test of models for lithospheric extension. Earth and Planetary Science Letters 234 (3–4), 401–419.
Crabaugh, M., Kocurek, G., 1993. Entrada Sandstone: an example of a wet aeolian system, 72. Geological Society, London. 1 Special Publications103–126.
Cruikshank, K.M., Aydin, A., 1995. Unweaving the joints in Entrada sandstone, Arches National Park, Utah, U.S.A. Journal of Structural Geology 17, 409–421.
Davatzes, N.C., Aydin, A., 2003. Overprinting faulting mechanisms in high porosity sandstones of SE Utah. Journal of Structural Geology 25, 1795–1813.
Davis, G.H., 1999. Structural geology of the Colorado Plateau Region of Southern Utah, with special emphasis on deformation bands. The Geological Society of America, 157 pp.
Dawers, N.H., Anders, M.H., Scholz, C.H., 1993. Growth of normal faults: displacement-length scaling. Geology 21 (12), 1107–1110.
Doelling, H.H., 2001. Geologic map of the Moab and eastern part of the San Rafael desert 30'x60' quadrangles, Grand and Emery Counties, Utah, and Mesa County, Colorado. Utah Geological Survey. Map 180.
Dreyer, T., Falt, L.M., Hoy, T., Knarud, R., Steel, R., Cuevas, J.L., 1993. Sedimentary architecture of field analogues for reservoir information (SAFARI); a case study of the fluvial Escanilla formation, Spanish Pyrenees. In: Flint, S.S., Bryant, I.D. (Eds.), The geological modelling of hydrocarbon reservoirs and outcrop analogues, vol. 15. Special Publication of the International Association of Sedimentologists, pp. 57–80.
Engelder, J.T., 1974. Cataclasis and the generation of fault gouge. GSA Bulletin 85, 1515–1522.
Evans, J.P., Forster, C.B., Goddard, J.V., 1997. Permeability of fault-related rocks, and implications for hydraulic structure of fault zones. Journal of Structural Geology 19, 1393–1404.
Faulkner, D.R., Jackson, C.A.L., Lunn, R.L., Schlische, R.W., Shipton, Z.K., Wibberley, C.A.J., Withjack, M.O., 2010. A review of recent developments concerning the structure, mechanics and fluid flow properties of fault zones. Journal of Structural Geology 32, 1557–1575.
Fisher, Q.J., Casey, M., Harris, S.D., Knipe, R.J., 2003. Fluid-flow properties of faults in sandstone: the importance of temperature history. Geology 31, 965–968.
Fisher, Q.J., Knipe, R.J., 1998. Fault sealing processes in siliciclastic sediments. In: Jones, G., Fisher, Q.J., Knipe, R.J. (Eds.), Faulting, Fault Sealing and Fluid Flow in Hydrocarbon Reservoirs, vol. 147. Geological Society, London, pp. 117–134. Special Publications.
Fisher, Q.J., Knipe, R.J., 2001. The permeability of faults within siliciclastic petroleum reservoirs of the North Sea and Norwegian Continental Shelf. Marine and Petroleum Geology 18, 1063–1081.
Flodin, E., Aydin, A., 2004. Faults with asymmetric damage zones in sandstone, Valley of Fire State Park, southern Nevada. Journal of Structural Geology 26, 983–988.
Fossen, H., 2010. Structural Geology. Cambridge University Press, New York, 463 pp.
Fossen, H., Bale, A., 2007. Deformation bands and their influence on fluid flow. AAPG Bulletin 91, 1685–1700.
Fossen, H., Hesthammer, J., 1997. Geometric analysis and scaling relations of deformation bands in porous sandstone. Journal of Structural Geology 19, 1479–1493.
Fossen, H., Hesthammer, J., 1998. Deformation bands and their significance in porous sandstone reservoirs. First Break 16, 21–25.
Fossen, H., Johansen, T.E.S., Hesthammer, J., Rotevatn, A., 2005. Fault interaction in porous sandstone and implications for reservoir management; examples from Southern Utah. AAPG Bulletin 89, 1593–1606.
Fossen, H., Schultz, R.A., Shipton, Z.K., Mair, K., 2007. Deformation bands in sandstone – a review. Journal of the Geological Society, London 164, 755–769.
Færseth, R.B., 2006. Shale smear along large faults: continuity of smear and the fault seal capacity. Journal of the Geological Society 163, 741–751. London.
Garden, I.R., Guscott, S.C., Burley, S.D., Foxford, K.A., Walsh, J.J., Marshall, J., 2001. An exhumed palaeo-hydrocarbon migration fairway in a faulted carrier system, Entrada Sandstone of SE Utah, USA. Geofluids 1 (3), 195–213.
Gawthorpe, R.L., Sharp, I., Underhill, J.R., Gupta, S., 1997. Linked sequence stratigraphic and structural evolution of propagating normal faults. Geology 25 (9), 795–798.
Harris, S.D., McAllister, E., Knipe, R.J., Odling, N.E., 2003. Predicting three-dimensional population characteristics of fault zones: a study using stochastic models. Journal of Structural Geology 25, 1281–1299.
Hesthammer, J., Bjørkum, P.A., Watts, L., 2002. The effect of temperature on sealing capacity of faults in sandstone reservoirs: examples from the Gullfaks and Gullfaks Sør fields, North Sea. AAPG Bulletin 86, 1733–1751.
Hesthammer, J., Fossen, H., 2000. Uncertainties associated with fault sealing analysis. Petroleum Geoscience 6, 37–45.
Hesthammer, J., Landrø, M., Fossen, H., 2001. Use and abuse of seismic data in reservoir characterisation. Marine and Petroleum Geology 18 (5), 635–655.
Hoffman, K.S., Taylor, D.R., Schnell, R.T., 1996. 3-D improves/speeds up fault plane analysis. Leading Edge 15, 117–122.
Howell, J.A., Vassel, Å, Aune, T., 2006. Modelling of dipping clinoform barriers within deltaic outcrop analogues from the Cretaceous Western Interior Basin USA 309. Geological Society, London, pp. 99–121. Special Publications.
Johansen, T.E.S., Fossen, H., Kluge, R., 2005. The impact of syn-faulting porosity reduction on damage zone architecture in porous sandstone: an outcrop example from the Moab Fault, Utah. Journal of Structural Geology 27, 1469–1485.
Kane, K.E., Jackson, C.A.L., Larsen, E., 2010. Normal fault growth and fault-related folding in a salt influenced rift basin: south Viking Graben, offshore Norway. Journal of Structural Geology 32, 490–506.
Kaproth, B.M., Cashman, S.M., Marone, C., 2010. Deformation band formation and strength evolution in unlithified sand: the role of grain breakage. Journal of Geophysical Research 115 (B12), B12103.
Kim, Y.-S., Peacock, D.C.P., Sanderson, D.J., 2004. Fault damage zones. Journal of Structural Geology 26, 503–517.
Knapp, R.W., 1990. Vertical resolution of thick beds, thin beds, and thin-bed cyclothems. Geophysics 55 (9), 1183–1190.
Knipe, R.J., 1993. The influence on fault zone processes and diagenesis on fluid flow. In: Horbury, A.D., Robinson, A.G. (Eds.), Diagenesis and Basin Development, vol. 36. AAPG Studies in Geology, pp. 135–154.
Knipe, R.J., 1997. Juxtaposition and seal diagrams to help analyze fault seals in hydrocarbon reservoirs. AAPG Bulletin 81, 187–195.
Kocurek, G., Robinson, N.I., Sharp, J.M., 2001. The response of the water table in coastal aeolian systems to changes in sea level. Sedimentary Geology 139 (1), 1–13.
Lindsay, N.G., Murphy, F.C., Walsh, J.J., Watterson, J., 1993. Outcrop studies of shale smears on fault surfaces. International Association of Sedimentologists Special Publication 15, 113–123.
Manzocchi, T., Walsh, J.J., Nell, P., Yielding, G., 1999. Fault transmissibility multipliers for flow simulation models. Petroleum Geoscience 5, 53–63.
Marchal, D., Guiraud, M., Rives, T., van den Driessche, J., 1998. Space and Time Propagation Processes of Normal Faults, vol. 147. Geological Society, London 1, pp. 51–70. Special Publications.
Marrett, R., Allmendinger, R.W., 1991. Estimates of strain due to brittle faulting: sampling of fault populations. Journal of Structural Geology 13 (6), 735–738.
McGrath, A.G., Davidson, I., 1995. Damage zone geometry around fault tips. Journal of Structural Geology 17, 1011–1024.
Micarelli, L., Moretti, I., Jaubert, M., Moulouel, H., 2006. Fracture analysis in the south-western Corinth rift (Greece) and implications on fault hydraulic behavior. Tectonophysics 426, 31–59.
Nuccio, V.F., Condon, S.M., 1996. Burial and thermal history of the Paradox Basin, Utah and Colorado, and Petroleum Potential of the Middle Pennsylvanian Paradox Basin. US Geological Survey, Reston, VA.
Peacock, D.C.P., Fisher, Q.J., Willlemse, E.J.M., Aydin, A., 1998. The relationship between faults and pressure solution seams in carbonate rocks and the implications for fluid flow. In: Jones, G., Fisher, Q.J., Knipe, R.J. (Eds.), Faulting, Fault Sealing and Fluid Flow in Hydrocarbon Reservoirs, vol. 147. Geological Society, London, pp. 105–115. Special Publications.
Peacock, D.C.P., Sanderson, D.J., 1991. Displacements, segment linkage and relay ramps in normal fault zones. Journal of Structural Geology 13, 721–733.

Pevear, D.R., Vrolijk, P.J., Longstaffe, F.J., 1997. Timing of Moab fault displacement and fluid movement integrated with burial history using radiogenic and stable isotopes. In: Hendry, J.P., Carey, P.F., Parnell, J. (Eds.), Geofluids II '97. Contributions to the second international conference on fluid evolution, migration and interaction in sedimentary basins and orogenic belts. Queen's University of Belfast, Belfast, pp. 10–14. March 1997, 42-45.

Rotevatn, A., Buckley, S.J., Howell, J.A., Fossen, H., 2009a. Overlapping faults and their effect on fluid flow in different reservoir types: a LIDAR-based outcrop modeling and flow simulation study. AAPG Bulletin 93. doi:10.1306/09300807092.

Rotevatn, A., Fossen, H., Hesthammer, J., Aas, T.E., Howell, J.A., 2007. Are relay ramps conduits for fluid flow? Structural analysis of a relay ramp in Arches National Park, Utah. In: Lonergan, L., Jolly, R.J.H., Sanderson, D.J., Rawnsley, K. (Eds.), Fractured Reservoirs, vol. 270. Geological Society, London, pp. 55–71. Special Publications.

Rotevatn, A., Tveranger, J., Howell, J.A., Fossen, H., 2009b. Dynamic investigation of the effect of a relay ramp on simulated fluid flow: geocellular modelling of the Delicate Arch Ramp, Utah. Petroleum Geoscience 15. doi:10.1144/1354-079309-779.

Schlische, R.W., 1995. Geometry and origin of fault-related folds in extensional settings. AAPG Bulletin 79 (11), 1661–1678.

Schlische, R.W., Young, S.S., Ackermann, R.V., Gupta, A., 1996. Geometry and scaling relations of a population of very small rift-related normal faults. Geology 24 (8), 683–686.

Scholz, C.H., Dawers, N.H., Yu, J.Z., Anders, M.H., Cowie, P.A., 1993. Fault growth and fault scaling laws: preliminary results. Journal of Geophysical Research 98 (B12), 21951–21961.

Shipton, Z.K., Cowie, P.A., 2003. A conceptual model for the origin of fault damage zone structures in high-porosity sandstone. Journal of Structural Geology 25, 333–344.

Shipton, Z.K., Evans, J.P., Robeson, K.R., Forster, C.B., Snelgrove, S., 2002. Structural heterogeneity and permeability in faulted aeolian sandstone: implication for subsurface modeling of faults. AAPG Bulletin 86, 863–883.

Shipton, Z.K., Evans, J.P., Thompson, L.B., 2005. The geometry and thickness of deformation-band fault core and its influence on sealing characteristics of deformation-band fault zones. In: Sorkhabi, R., Tsuji, Y. (Eds.), Faults, Fluid Flow and Petroleum Traps, vol. 85. AAPG Memoir, pp. 181–195.

Solum, J.G., van der Pluijm, B.A., Peacor, D.R., 2005. Neocrystallization, fabrics and age of clay minerals from an exposure of the Moab Fault, Utah. Journal of Structural Geology 27 (9), 1563–1576.

Sorkhabi, R., Tsuji, Y., 2005. Faults, fluid flow and petroleum traps. AAPG Memoir 85, 342.

Sperrevik, S., Færseth, R.B., Gabrielsen, R.H., 2000. Experiments on clay smear formation along faults. Petroleum Geoscience 6 (2), 113–123.

Stephen, K.D., Dalrymple, M., 2002. Reservoir simulations developed from an outcrop of incised valley fill strata. AAPG Bulletin 86, 797–822.

Sverdrup, E., Bjørlykke, K., 1997. Fault properties and the development of cemented fault zones in sedimentary basins. In: Møller-Pedersen, P., Koestler, A.G. (Eds.), Hydrocarbon Seals: Importance for Exploration and Production, vol. 7. Norwegian Petroleum Society, pp. 91–106. Special Publication.

Trudgill, B.D., 2010. Evolution of salt structures in the northern Paradox Basin: controls on evaporite deposition, salt wall growth and supra-salt stratigraphic architecture. Basin Research (no-no).

Trudgill, B.D., Cartwright, J.A., 1994. Relay ramp forms and normal fault linkages, Canyonlands National Park, Utah. GSA Bulletin 106, 1143–1157.

Walsh, J.J., Watterson, J., 1988. Analysis of the relationship between displacements and dimensions of faults. Journal of Structural Geology 10 (3), 239–247.

Walsh, J.J., Watterson, J., Heath, A.E., Childs, C., 1998. Representation and scaling of faults in fluid flow models. Petroleum Geoscience 4, 241–251.

Wibberley, C.A.J., Petit, J.-P., Rives, T., 2000. Mechanics of cataclastic 'deformation band' faulting in high-porosity sandstone, Provence. Comptes Rendus de l'Académie des Sciences 331, 419–425.

Withjack, M.O., Olson, J., Peterson, E., 1990. Experimental models of extensional forced folds. AAPG Bulletin 74 (7), 1038–1054.

Yielding, G., Freeman, B., Needham, D.T., 1997. Quantitative fault seal prediction. AAPG Bulletin 81, 897–917.